machines

MDPI

Article

Optimization of the Screw Conveyor Device Based on a GA-BP Neural Network

Qiang Guo [1,2,*], Yunpeng Zhuang [1], Houzhuo Xu [1], Wei Li [1], Haitao Li [3] and Zhidong Wu [1]

1 College of Mechanical and Electrical Engineering, Qiqihar University, Qiqihar 161000, China; zyp20000219@163.com (Y.Z.); xhzjixie@163.com (H.X.); l1486336673@163.com (W.L.); wzd139446@163.com (Z.W.)
2 The Engineering Technology Research Center for Precision Manufacturing Equipment and Industrial Perception of Heilongjiang Province, Qiqihar 161000, China
3 Heilongjiang Provincial Academy of Agricultural Machinery Engineering Sciences, Qiqihar 161000, China; haitao348065412@126.com
* Correspondence: gq_jixie@163.com

Abstract: As technology advances, so does digital farming, revolutionizing the industry. Drones, sprayers equipped with GPS and other sensors, combine harvesters, and other machinery can greatly improve agricultural productivity. This paper studies the impact of the straw baler screw conveyor on the efficiency of the baler. Via theoretical analysis, GA—BP (Genetic Algorithm—Back Propagation) simulation, and comparative experiments, the structural parameters and rotational speed of the spiral shaft in the screw conveying device are optimized. In this paper, we analyze the force and velocity components acting on the straw, give the design principles for the screw's conveying parameters under the premise of ensuring maximum conveying capacity and minimum power consumption, and determine the optimal design variables, objective functions, and constraints according to the specific optimization problem; we establish a specific mathematical model, and introduce algorithm optimization for nonlinear problems with many variables and large amounts of calculations. In MATLAB, an optimization calculation and analysis were performed. The optimization results of the traditional BP (Back Propagation) and GA—BP were compared. It was proven that GA—BP could effectively compensate for the deficiencies of the BP neural network and substantially enhance the model's accuracy. Through an analysis of the optimization results, the conclusion of attaining the optimization objective was drawn. Specifically, when the outer diameter of the spiral for screw conveyance in the straw baler was D = 320 mm, the pitch was S = 200 mm, and the rotational speed of the pickup shaft was $n = 138\ r/\mathrm{min}$, the straw baler could achieve the maximum conveying capacity and the minimum power consumption. At this moment, the power consumption was P = 0.079 kW, and the conveying capacity was $Q_m = 23.98$ t/h. Subsequently, the optimization results were contrasted with those of other mainstream domestic models, and a comparative experiment was conducted. The experimental results indicated that the model's prediction results were reliable and exhibited higher efficiency compared to other combinations. The results could provide a reference for the research on screw conveyance of balers.

Keywords: digital farming; screw conveyor; BP neural network; GA-BP algorithm

Academic Editor: Dan Zhang

Received: 27 November 2024
Revised: 26 December 2024
Accepted: 31 December 2024
Published: 1 January 2025

Citation: Guo, Q.; Zhuang, Y.; Xu, H.; Li, W.; Li, H.; Wu, Z. Optimization of the Screw Conveyor Device Based on a GA-BP Neural Network. *Machines* **2025**, *13*, 24. https://doi.org/10.3390/machines13010024

1. Introduction

In China, the cultivated land area is extensive, and the production of straw crops is substantial with a diverse range of varieties. The straw is rich in fiber, organic substances, and essential elements for crop growth [1]. Simultaneously, it can be recycled back to the field, thereby fulfilling the functions of enhancing soil fertility, sequestering carbon, and ameliorating soil structure [2,3]. Only highly efficient automated mechanical equipment can furnish the requisite support and assurance for the comprehensive utilization of corn straw resources. Four main components make up the baler: a pickup mechanism, a feeding mechanism, a cutting mechanism, and a baling mechanism. The performance of the feeding mechanism directly mirrors the quality of the baler [4]. The screw conveying component dictates the performance of the feeding mechanism. Consequently, screw conveying exerts a crucial influence on the performance of the baler [5]. Research on balers has been in progress for several decades and has attained numerous achievements [6].

Wang Qingqing et al. [7] constructed a simulation model of a straw picker using the ADAMS-DEM (Automatic Dynamic Analysis of Mechanical Systems-Discrete Element Method) coupling method, and conducted verification tests in the field for different forward speeds and straw coverage rates. Tang Zhong et al. [8] have developed a crawler-type picking and baling machine. Based on the conceptual model of the crawler-type picking and baling machine, the working principle and parameter model have been analyzed, and a structural design model has been established. Kalay E et al. [9] adopted the Design of Experiments (DOE) approach to optimize the parameters of an Artificial Neural Network (ANN) by significantly reducing the number of virtual experiments. Moreover, single spheres and clumped spheres were utilized to consider the impact of particle shape on the mass flow rate. After being trained, the Artificial Neural Network was able to accurately and efficiently predict the mass flow rate by taking both the parameters related to screw conveyors and those related to granular particles as inputs. Zhao Zhan et al. [10] used the Discrete Element Method (DEM) to simulate the feeding process of straw and designed a hydraulic cylinder drive circuit with an accumulator. A straw bale experiment was carried out, and its performance was basically consistent with the DEM simulation. Hu Baichen [11] designed a peanut-picking and -harvesting long seedling-conveying and -collecting device; using the CFD-DEM (Computational Fluid Dynamics-Discrete Element Method) coupled simulation method, the device was studied. Li G et al. [12], by employing the Response Surface Methodology (RSM) for solution exploration and the Genetic Algorithm (GA) integrated within the Artificial Neural Network (ANN) model for GA-based computation, conducted a detailed comparison of crucial parameters. The results reveal that the static friction coefficient between silage and silage, the rolling friction coefficient between silage and silage, as well as the static friction coefficient between silage and the steel body are all significant factors exerting a profound impact on the stacking angle throughout the stacking process. Ye Tian et al. [13] proposed a new type of screw conveyor with flexible discrete helical blades. Through theoretical analysis, a power consumption model of a screw conveyor with flexible discrete helical blades was established. Its practicality was verified through simulation and experimental testing.

Many researchers have long overlooked the influence of spiral conveying on balers, resulting in a paucity of in-depth investigations into this crucial aspect of baler operation. Complicating matters further is the multitude of variables that impact the efficiency of spiral conveying, which renders the task of conducting comprehensive combinatorial optimization exceedingly challenging. Furthermore, optimizing the conveying capacity and power consumption as key performance indicators has received scant attention. As a consequence, the spiral conveying apparatuses within agricultural straw balers continue to grapple with persistent issues, namely, excessive power consumption and a relatively low conveying rate, which significantly impede the overall performance and energy efficiency of these machines.

In this paper, the methods of theoretical analysis and algorithm simulation are employed to analyze and optimize the performance of the screw conveying device. Through analysis, the factors influencing conveying capacity are determined, and mathematical models of power consumption and conveying capacity are formulated. By utilizing MATLAB (R2023a) software to develop programs and combining the genetic algorithm with GA—BP on the foundation of the traditional BP algorithm, the screw conveying device is optimized to obtain the optimized parameter combination that maximizes conveying capacity and minimizes power consumption. Comparative experiments are also carried out to provide a reference for research on the screw conveying device of the baler.

2. Materials and Methods

Figure 1 displays the whole process of optimizing the screw conveying components of the straw baler. It aims to clearly show the logical relationships between all the links, starting with explaining how the straw baler works and the structure of screw conveying and ending with conducting experiments and drawing conclusions.

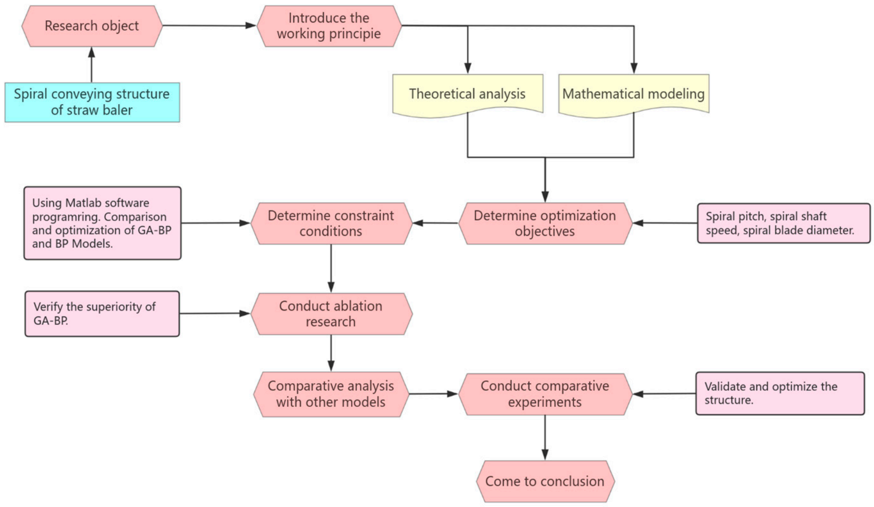

Figure 1. Research process of the article.

2.1. Working Principle of Straw Balers

Today, in almost all agricultural auxiliary machines (presses, seeders, mineral fertilizer dispensers, straw balers, potato diggers, etc.) torque and power of the tractor is mainly transmitted mechanically through the cardan shaft [14,15].

The overall structure of the round baler mainly completes the operations of picking, feeding, bundling, and bale unloading [16,17]. The main components of the round baler are the transmission system, pick-up, feeding mechanism, bale chamber, and bale unloading device [18,19]. Figure 2 illustrates the overall structure. When fieldwork is carried out, the tractor transmits power to various components through the power system. The pick-up device collects straw that is scattered in the field and feeds it into the bale chamber through the screw conveyor and other feeding components. Due to the presence of the rotating drum, the straw is gradually rotated into a bale. The machine keeps working, winding the straw around the growing bale until the bale unloading device finally unloads it.

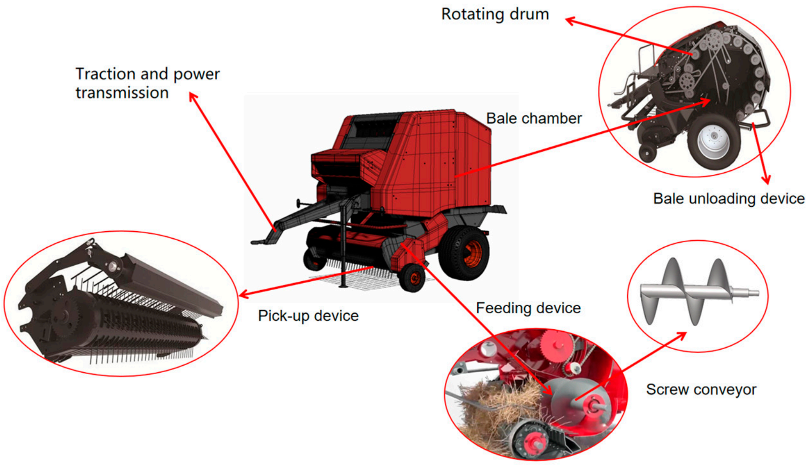

Figure 2. Model of baler and schematic diagram of work.

2.2. Analysis of the Overall Structure of the Screw Conveyor

The Helix Angle

The spiral blade constitutes the principal component of the spiral conveying device and manifests in diverse forms, namely the full-surface-type, belt-type, toothed-type, and paddle-type. In the context of this research, a solid spiral blade with a positive helix was chosen [20,21]. The rationale behind this selection lies in the fact that the spiral conveying mechanism of the straw baler is chiefly tasked with transporting light, regularly shaped, and low-density straw and fodder crops.

The angle between the normal of any point on the spiral blade and the axis of the helix is referred to as the helix angle φ at that point, which is determined by Equation (1).

$$\varphi = \tan^{-1}\left(\frac{S}{\pi D_i}\right) \tag{1}$$

where S is the screw pitch, mm, and D_i is the diameter of a spiral blade at a certain point, mm.

2.3. Mechanical Analysis of Straw

For the sake of analysis, the straw is considered a particle, and one side of the spiral conveyor is considered a slash. According to Figure 3, if the picking mechanism picks up the straw during operation and throws it to point O on the helix surface under the action of the spring-teeth, and the straw's absolute speed at the point of contact with the helix surface is zero. Therefore, the straw experiences a normal thrust on the spiral surface, along with a tangential upward frictional force f. Force F produces a deflection force F_1, which decomposes into axial force F_x and radial force F_y under the action of friction force f. The straw is transported in the axial direction under the action of the axial force F_x. If the axial force F_y and the friction force f acting on the straw are too large and greater than the force of gravity G and the friction force generated by the contact between the helix surface and the straw, the straw will rotate with the helix shaft and will not be transported well in the axial direction.

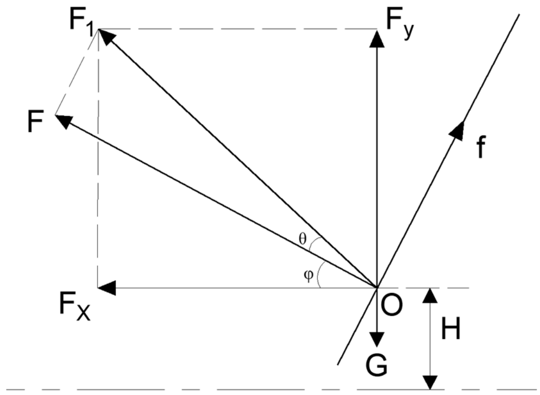

Figure 3. Schematic diagram of stress forces on straw.

Therefore, the magnitude of F_x, F_y, and the friction force f can be derived as

$$\begin{cases} F_{\mathrm{x}} = F_1 \cos(\varphi + \theta) \\ F_{\mathrm{y}} = F_1 \sin(\varphi + \theta) \end{cases} \tag{2}$$

$$f = F \tan\theta = F\mu \tag{3}$$

From Equation (1), it follows that $\varphi = \tan^{-1}\left(\frac{S}{\pi H}\right)$, and $\theta = \tan^{-1}\mu$.

Where μ is the coefficient of friction between the straw and the spiral surface and H is the radius of the position where the straw is located at point O.

Since the friction force f is the force that prevents the straw from moving laterally, it can be seen from the figure that if the straw is to be moved laterally, it must be ensured that the radial component of the normal thrust is less than the axial component, i.e.,

$$F \cos\varphi > f \sin\theta \tag{4}$$

Solving Equations (3) and (4) simultaneously gives

$$F \cos\varphi > F \tan\theta \sin\theta \tag{5}$$

Therefore, for the straw to be transported successfully, $\varphi < \frac{\pi}{2} - \theta$ must be satisfied. The analysis shows that the closer the particle is to the helix axis, the greater the helix angle, and that as the helix angle increases, the axial force F_x gradually decreases. As the radial force F_y increases, so does the rotational force on the straw. When the radial force F_y reaches a certain level, the straw will rotate with the spiral shaft instead of being transported in the axial direction. This will not only waste power but also cause the conveying device to block, thereby affecting the efficiency of the entire device. In addition, the basic parameters of the screw conveying mechanism also affect the conveying efficiency.

2.4. Kinematic Analysis

As shown in Figure 4, we can observe that when the baler is working, the screw conveyor rotates at an angular speed ω, so the straw at point O will have a linear speed V_2 in the direction of the tangent of this point. Ignoring friction, the straw will move along the normal direction of the spiral blade at a speed of V. However, due to friction between the straw and the spiral blade, the speed V will be offset by a speed V_1. The speed V_1 can be decomposed into an axial speed V_x and a circumferential speed V_y. The lateral speed, the axial speed V_x, is the straw conveying speed, while the circumferential speed V_y hinders the straw conveying. According to the triangle inequality, it follows that

$$\begin{cases} V_x = V_1 \cos(\varphi + \theta) \\ V_y = V_1 \sin(\varphi + \theta) \end{cases} \tag{6}$$

among them

$$\begin{cases} V = \frac{V_1}{\cos\theta} = \frac{V_2 \sin\varphi}{\cos\theta} \\ V_2 = \omega H = \frac{2\pi n}{60} H_1 \end{cases} \tag{7}$$

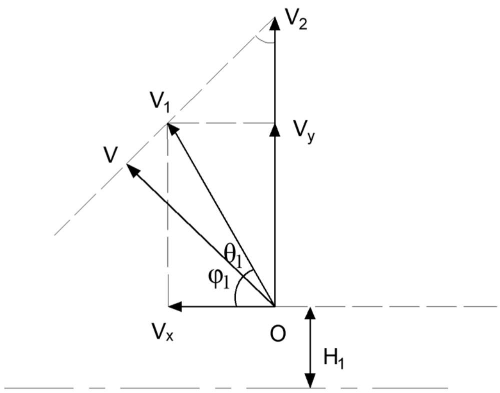

Figure 4. Schematic diagram of straw kinematics.

According to the derivation formula of the pitch, there is

$$H_1 = \frac{S}{2\pi \tan\varphi} \tag{8}$$

Then

$$V_2 = \frac{2n\pi}{60} \times \frac{S}{2\pi \tan\varphi} = \frac{nS}{60 \tan\varphi} \tag{9}$$

Therefore

$$V = \frac{nS}{60 \tan\varphi} \times \frac{\sin\varphi}{\cos\theta} = \frac{nS \cos\varphi}{60 \cos\theta} \tag{10}$$

Due to

$$\begin{cases} \cos\varphi = \frac{1}{\sqrt{(\tan\varphi)^2 + 1}} \\ \sin\varphi = \frac{\tan\varphi}{\sqrt{(\tan\varphi)^2 + 1}} \end{cases} \tag{11}$$

The analysis in Section 2.2 shows that $\varphi = \tan^{-1}\left(\frac{S}{\pi H}\right)$, and $\theta = \tan^{-1}\mu$; therefore, by combining Formulas (6), (10) and (11), it can be obtained that

$$\begin{cases} V_x = \frac{nS}{60} \times \frac{1 - \frac{\mu S}{2\pi H_1}}{\left(\frac{S}{2\pi H_1}\right)^2 + 1} \\ V_y = \frac{nS}{60} \times \frac{\frac{S}{2\pi H_1} + \mu}{\left(\frac{S}{2\pi H_1}\right)^2 + 1} \end{cases} \tag{12}$$

where n is the spiral axis speed, r/min; V_x is the transverse speed of the straw, m/s; V_y is the radial velocity of the straw, m/s; and H_1 is the radius of the position where the straw is located at point O.

3. Parameter Determination for Screw Conveying

3.1. Spiral Diameter

Most domestic and foreign spirals have standardized their diameter. There are a lot of popular balers on the market, such as the New Holland 850 round baler pickup device (It is produced by CNH Industrial (Case New Holland) in the United States), the 5120/5120K round baler (It is produced by Sinomach Mino Company in China), the 9JK-1.7 baler pickup device (It was developed by the Chinese Academy of Agricultural Sciences), and the 4YZK-4 square baler pickup and baling device (made by the Qiqihar branch of Heilongjiang Agricultural Machinery College). The diameter of the auger is between 300 mm and 400 mm. Therefore, the outer diameter of the helix should meet 300 mm $\leq D \leq$ 400 mm.

3.2. Helical Axis Speed

Generally speaking, there is a positive correlation between the speed of the auger shaft and the conveying capacity, that is, the higher the speed of the auger shaft, the greater the conveying capacity. However, when the screw shaft reaches a specific critical speed, excessive centrifugal force will act on the straw, pushing it outwards. Given the auger feeding structure of the baler, such a phenomenon will trigger straw blockages, which will not only severely impede production efficiency but may also reduce the service life of the machine. Conversely, if the speed of the screw shaft is overly low, the material cannot be transported in an efficient manner. Moreover, as the picking mechanism continuously gathers straw, the straw will accumulate and clog the screw conveyor. Thus, it is essential to impose a speed limit and determine an optimal value. In practical operation, for the straw to be transported smoothly, the gravitational force of the straw itself must exceed the centrifugal force generated by the rotation of the screw axis. From this, the following conditions or equations can be derived.

$$\begin{cases} mg \geq m\omega_{\max}^2 R \\ \omega = \frac{2\pi n}{60} \end{cases} \tag{13}$$

can be

$$n_{\max} \leq \frac{30}{\pi}\sqrt{\frac{g}{R}} \leq \frac{30}{\pi}\sqrt{\frac{2g}{D}} \tag{14}$$

Taking into account the characteristics of different straws, we can

$$n_{\max} \leq \frac{30K}{\pi}\sqrt{\frac{2g}{D}} \tag{15}$$

where K is the overall coefficient of materials; g is gravitational acceleration, m/s^2; and $n_{\max}$ is the maximum speed of the screw axis. A straw baler is mainly used for harvesting crops such as wheat and corn. According to Table 1, the K value is 0.0558 and the regularity is 0.05. Bringing this into Equation (15) gives $n_{\max} \leq \frac{3\pi}{2}\sqrt{\frac{2g}{D}}$.

Table 1. Different material properties.

Size of a Block	Example	Filling Factor	K
Powder	Flour, Rice flour	0.40~0.50	0.0387
Powder	Cement, Lime	0.30~0.40	0.0415
Granular	Sandstone, Chemical fertilizer	0.20~0.35	0.0632
Lump	Wheat, Corn	0.25~0.30	0.0558
Lump	Soybean meal, Vegetable cake	0.30~0.35	0.5940
Lump	Coal, Ore	0.15~0.20	0.0795
Liquid	Dough, Paper pulp	0.55~0.60	0.0785
Liquid	Concrete, Building material	0.50~0.55	0.0654

3.3. Screw Pitch

The size of the screw pitch determines the helix angle. Equation (2) reveals that the screw pitch size influences the force component acting on the straw during transport. Therefore, the size of the screw pitch directly affects the conveying efficiency of the entire machine. Once the outer diameter of the screw and the conveying capacity are determined, changes in the pitch will lead to alterations in the transverse movement plane of the straw, thereby affecting the component velocities of the straw's movement. Therefore, the most reasonable screw pitch size should be determined based on the relationship between the spiral surface and straw friction, as well as the appropriate distribution relationship between the velocity components.

(1) The relationship between the spiral surface and the friction of the straw

According to the above analysis, if the straw moves laterally, $\varphi < (\frac{\pi}{2} - \theta)$ must be satisfied. Additionally, if the lateral component of the straw's force is greater than 0, then $F_x = F_1 \cos(\varphi + \theta) > 0$ is satisfied. During screw transportation, the helix angle is smaller the closer it is to the outer edge of the screw blade and the largest when it is closest to the screw axis, when $H_1 = \frac{d}{2}$ (where d is the diameter of the screw axis). The helix angle is maximum, and the lateral component F_x of the straw force is minimum at this time. Therefore, according to Equation (1), the maximum critical value of the screw pitch is $S_{\max} \leq \pi d \tan(\frac{\pi}{2} - \theta) = \frac{\pi d}{\tan\theta}$. Let $d = K_1 D$ (K_1 is the screw axis diameter factor, taken as $K_1 = 0.5$), then $S_{\max} \leq \pi K_1 D \tan(\frac{\pi}{2} - \theta) = \frac{\pi d}{\tan\theta}$.

(2) The distribution relationship between the speed components

The size of the screw pitch affects the relationship between the speed components. Increasing the screw pitch leads to an increase in the transverse and radial speeds of the straw. Reducing the screw pitch improves the distribution of the speed components, but it also reduces the transverse conveying speed, thereby affecting the baler's efficiency. Therefore, when determining the screw pitch, while satisfying the premise of a good distribution of each speed component, it is necessary to satisfy the condition that the lateral speed is greater than the radial speed, i.e., $V_x > V_y$, and also make the lateral speed as large as possible, so that:

$$\frac{nS}{60} \times \frac{1 - \frac{\mu S}{2\pi H_1}}{(\frac{S}{2\pi H_1})^2 + 1} > \frac{nS}{60} \times \frac{\frac{S}{2\pi H_1} + \mu}{(\frac{S}{2\pi H_1})^2 + 1} \tag{16}$$

We can rearrange the formula to get $S \leq 2H_1 \tan(\frac{\pi}{4-\theta})$. At the outer diameter $2H_1 = D$ of the helix, the maximum critical value of the screw pitch is $S_{\max} \leq 2\pi D \tan(\frac{\pi}{4-\theta})$, so the screw pitch should meet the following two conditions.

$$\begin{cases} S_{\max} \leq \pi K_1 D \tan(\frac{\pi}{2} - \theta) \\ S_{\max} \leq 2\pi D \tan(\frac{\pi}{4-\theta}) \end{cases} \tag{17}$$

3.4. Screw Conveying Power

The total power of the screw conveyor mechanism includes the power P_1 of the machine running without load and the power P_2 when working. The baler screw conveyor conveys horizontally, so the power in the inclined state is not considered. The following formula can be

$$P_1 = \frac{DL}{20},\ P_2 = \frac{Q_{\mathrm{m}} L \gamma}{367}$$

where Q_m is the mass throughput, kg; D_{i} is the spiral outer diameter, m; L is the conveying distance, m; and γ is running resistance coefficient. γ is defined as 0.5.

3.5. Screw Conveyor Conveying Capacity

Conveying capacity is an indicator of the quality of the conveying mechanism and one of the criteria for measuring the operating efficiency of the baler. The screw pitch, rotational speed, and the cross-sectional area of the straw in the screw conveying mechanism influence the conveying capacity during the actual design process. The formula in the literature allows for the calculation of conveying capacity.

$$Q_m = 3600 A V \rho \tag{18}$$

where A is the cross-sectional area of straw in the screw conveyor, mm^2; V is the speed of straw transport, m/s; and ρ is the bulk density of the straw, $\mathrm{kg/m}^3$.

The bulk density of straw of different qualities also varies to a certain extent. According to the characteristics of crops in Heilongjiang Province, ρ is defined as 120 $\mathrm{kg/m}^3$. Ignoring the axial blockage of the straw in the conveying mechanism, the following formula can be obtained $A = \frac{\pi D_{\mathrm{i}} \delta}{4}$, $V = \frac{\mathrm{Sn}}{60}$. Substituting this into Equation (11) gives,

$$Q_{\mathrm{m}} = 15 \pi D_{\mathrm{i}}^2 \delta S \mathrm{n} \tag{19}$$

where δ is filling factor.

In order to achieve the best conveying performance and maximize the efficiency of the baler, it is necessary to achieve the highest efficiency and lowest energy consumption of the conveying mechanism. As can be seen from Equation (7), the conveying capacity of the screw conveying device is proportional to the square of the outer diameter of the screw D_{i}^2, the screw pitch S, and the speed of the screw axis n. To achieve high productivity, the screw pitch and speed must be large; however, to achieve low energy consumption, it is necessary to achieve low speed and small feed conditions and find the appropriate screw pitch.

$$\max g(x) = \frac{Q_m}{P} = \frac{0.15 Q_m}{367} + 0.025 = 1.884 D_i S n + 2.45 \tag{20}$$

The corresponding objective function is therefore

$$g(x) = 2.45 + 1.884 x_1 x_2 x_3 \tag{21}$$

3.6. The Constraint Conditions

$x_1 x_2 x_3$ represent the outer diameter of the helix, screw pitch, and rotational speed, respectively. Based on the analysis above, the mathematical constraints are determined and should be met during the MATLAB (R2023a) optimization process.

$$f_1(x) = x_1 > 300 \tag{22}$$

$$f_2(x) = x_1 < 400 \tag{23}$$

$$f_3(x) = x_3 - \frac{3\pi}{2}\sqrt{\frac{2g}{x_1}} \leq 0 \tag{24}$$

$$f_4(x) = x_2 - \frac{1}{2}\pi x_1 \tan(\frac{\pi}{2} - \theta) = x_2 - \frac{\pi x_1}{\mu} \leq 0 \tag{25}$$

$$f_5(x) = x_2 - 2\pi x_1 \tan(\frac{\pi}{4-\beta}) = x_2 - \frac{\pi x_1(1-\mu)}{1+\mu} \leq 0 \tag{26}$$

4. Genetic Algorithm-Based Optimization of BP Neural Networks

4.1. BP Neural Network Algorithm Implementation

Since the 1980s, neural networks have emerged as a prominent research focus within the realm of artificial intelligence [22,23]. They abstract the neural network of the human brain from an information-processing perspective, constructing a particular simplistic model and assembling diverse networks through varying connection modalities [24,25]. In both engineering and academic circles, they are commonly abbreviated as neural networks or neural-like networks, serving as a potent instrument for addressing nonlinear problems. The text conducts an analysis to formulate the objective function, constraint function, and perform variable analysis, with the utilization of MATLAB(R2023a) software for program writing.

The structure of the BP neural network model is shown in Figure 5.

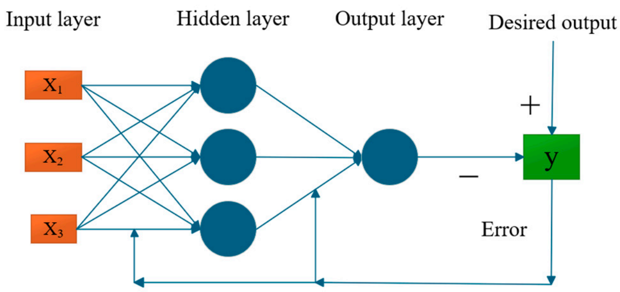

Figure 5. BP neural network structure diagram.

1. The leftmost part is called the input layer, the middle part is called the hidden layer, and the rightmost part is called the output layer;

2. Neurons in the same layer are not connected;

3. Each neuron in the Nth layer is connected to all neurons in the $(N-1)$th layer (this is the meaning of "Full connected"). The output of the $(N-1)$th layer neurons is the input of the Nth layer neurons;

4. Each neuron connection has a weight value. It should be noted that here, X = (x_1,x_2,x_3) and represents an input vector, and y represents an output vector.

Adding hidden layers can reduce network errors and improve accuracy, but it also complicates the network, increasing training time and potentially leading to overfitting [26,27]. Increasing the number of nodes in the hidden layer can result in fewer errors, and this training effect is easier to achieve than increasing the number of hidden layers. Therefore, according to the empirical formula, the number of nodes (n_1) in the hidden-layer neural grid is:

$$n_1 = \sqrt{n+m} + a \tag{27}$$

where n_1 is the number of hidden layer nodes; m is the number of input layer nodes; n is the number of output layer nodes; and a is the adjustment constant between 1 and 10.

The number of neurons in the input layer corresponds to the number of input variables in the processed data, while the number of neurons in the output layer corresponds to the number of outputs linked to each input. Analysis in accordance with Section 3 could determine that $m = 3$, $n = 1$. To reduce errors, we set $a = 10$ and $n_1 = 12$.

The transfer function of the neurons in the hidden layer of the neural network uses the S-type tangent function, and the transfer function of the neurons in the output layer uses the S-type logarithmic function, because the 0–1 output mode is required for the network output.

4.2. Network Training and Testing

Network training is a process of continuously modifying weights and thresholds. Through training, the output error becomes smaller and smaller. The analysis in 3.6 states that a function randomly generates 100 sets of data, 90 of which are for the training set and 10 for the test set, using $x_1 x_2 x_3$ (spiral outer diameter, pitch, and rotational speed) as the input variables and $g(x)$ as the output variable. The network parameters were set as follows: The number of training times was 1000, the training target was 1×10^{-6}, the optimization algorithm selected was stochastic gradient descent, the learning rate was 0.01, and the batch size was 256 to ensure a good balance between training speed and model convergence. The regularization parameter was 0.3. Figure 6 displays the results after running the code.

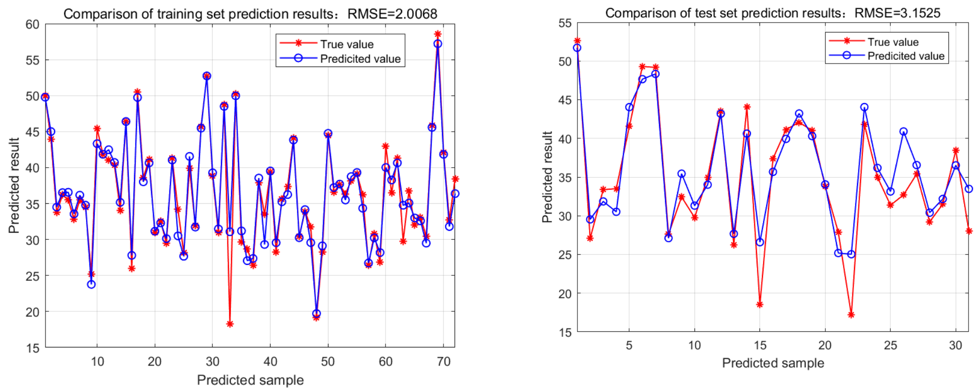

(**a**) (**b**)

Figure 6. BP neural network verification analysis chart. (**a**) Results of the training set; (**b**) results of the test set.

We used the function to randomly generate 100 sets of data, including 90 training sets and 10 test sets. After training the model, we proceeded with data processing on the randomly selected test samples to standardize the data. After the simulation, the output value of the test sample was obtained, and the reliability of the model was judged by comparing the difference between the output value and the expected output value. As shown in Figure 6, the predicted value basically overlapped with the verified value, indicating that the predicted value was consistent with the verified value, but individual predicted values differ from the actual values. The root mean square errors (RMSE) of the test set and training set was 3.1525 and 2.0068, respectively.

Figure 7 reveals that the model's lowest correlation coefficient (R) was 0.916, while its overall correlation coefficient (R) stood at 0.965. The model's predicted values fit the training values well, but the root mean square error of the test set was 3.152, which is relatively large.

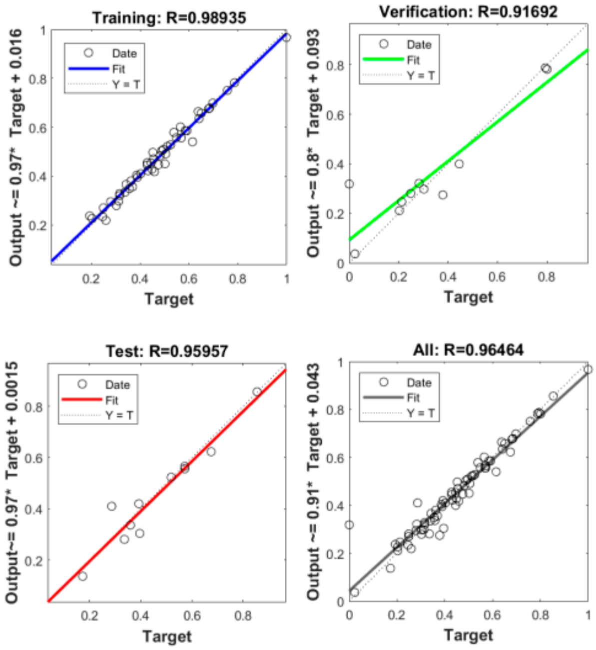

Figure 7. BP neural network regression. The asterisk (*) indicates that the P-value of the model is less than 0.05, which proves that the model is reliable.

4.3. Genetic Algorithm Optimization of BP Neural Networks

The BP algorithm randomly generates its initial solution [27]. Despite its outstanding prowess in resolving nonlinear problems, the randomness of this initial solution impacts the algorithm's performance, rendering it unstable. It adopts the gradient descent method to determine the search direction. In the search space, flat zones and multiple local minima exist, causing the algorithm to be vulnerable to slow convergence or failure to converge as it may get stuck in a local minimum [28,29].

In the 1970s, the American John Holland introduced genetic algorithms, inspired by biological evolution laws. These algorithms employ mathematics and computer simulations to mimic the biological process of chromosomes crossing and evolving over time for problem-solving. When handling more intricate combined optimization problems, genetic algorithms often outpace some traditional optimization algorithms, more swiftly achieving better optimization results. Within a population, multiple individuals concurrently conduct a global search, which ensures the ultimate discovery of the optimal model. Genetic algorithms also exhibit excellent performance in global search tasks [29].

In this scenario, the multiple and non-linear optimization objectives necessitate the use of genetic algorithms to determine the optimal network weights and thresholds, which serve as the initial values for the subsequent neural network model. This fixes the problem with regular BP neural networks, that they can reach local minima, and it also makes model evaluation a lot more accurate.

(1) Coding method

In our research, a binary coding method was adopted. Under this method, each individual within the system was designed to hold the network parameters. Specifically, weights were incorporated in each of the input layer, hidden layer, and output layer, while thresholds were only present in the hidden and output layers.

Genetic algorithms function based on a population composed of N individuals, with the algorithmic efficiency hinging on the specific value of N. As documented in the relevant literature, the typical range for N is from 10 to 200. To enhance the diversity of the population and preclude the emergence of identical individuals, separate operations were conducted on each individual. Consequently, the expression of an individual could be represented as $X_i = (a_1, a_2, a_3 \ldots a_{113}), i = 1, 2, 3, \ldots, N$.

(2) Determining the fitness function. We used the screw-conveyor power consumption and screw-conveyor volume as a fitness function and scored the fitness function using a ranking method.

(3) Mutation operation. This operation makes each gene a point of variation and then randomly selects a value within the range of values to replace the original value.

(4) Cross-operate. Populations underwent linear recombination. Suppose there was a linear recombination between A and B. Then the new individual after crossing was:

$$\begin{cases} X_i^{t+1} = aX_j^t + (1-a)X_i^t \\ X_j^{t+1} = aX_i^t + (1-a)X_j^t \end{cases}$$

(5) Parameter setting. The roulette wheel method served as the selection strategy, the population type was a real vector, the population size was 100, and the number of iterations reached served as the termination condition. The number of iterations was 200.

4.3.1. GA-BP Algorithm Process

As shown in Figure 8, it is the flowchart of the GA-BP algorithm.

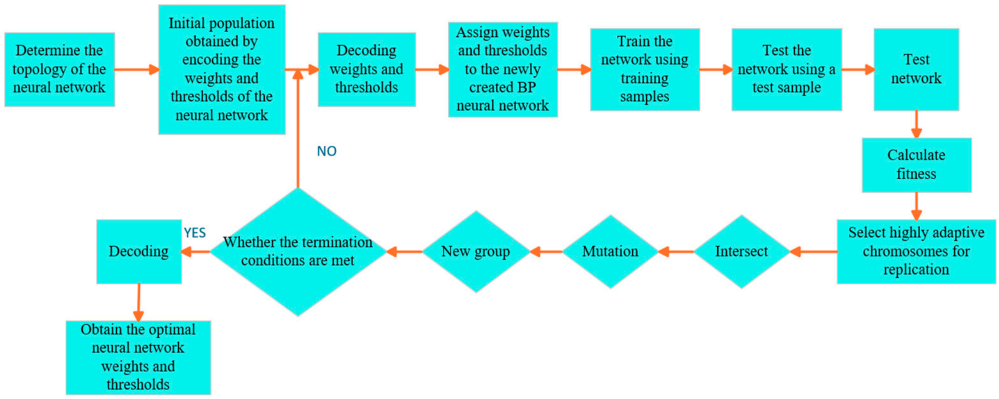

Figure 8. Flowchart of GA-BP algorithm.

4.3.2. Analysis of Experimental Results

In this experimental investigation, a comprehensive comparison was meticulously conducted between the outcomes yielded by the genetic algorithm-optimized BP model (GA-BP) and those of the conventional BP model. Tables 2 and 3 distinctly illustrate the parameter configurations for the BP model and the GA-BP model respectively, affording a lucid visualization of the specific settings adopted in each case.

Table 2. BP neural network parameter settings.

Number of Training Sessions	Training Target	Learning Rate	Training Function	Transfer Function
1000	1×10^{-6}	0.01	trainlm	tan-sigmoid

Table 3. GA-BP parameter settings.

Population Size	Probability of Mutation	Number of Iterations	Cross-Probability
100	0.1	200	0.3

The genetic algorithm optimizes the initial weight and threshold matrix. You can verify the performance indicators of the GA-BP model prediction value using the initial weight and threshold. The actual compensation value output result of the GA-BP model in the training set and the absolute error between the predicted GA-BP model compensation value and the actual value were selected. During the analysis of these two performance indicators, the prediction results of the traditional BP model were also selected for comparison, aiming to further confirm the stability and reliability of GA–BP.

As shown in Figure 9, the GA-BP algorithm fitness function is the sum of the absolute values of the training errors of all samples. Therefore, the overall trend of fitness should decrease as the number of generations increases. Upon reaching 200 generations, the mean individual fitness stabilized, suggesting that the preset maximum number of evolutions was reasonable and the genetic algorithm could produce the optimal solution for BP neural network weight and threshold adjustment within a reasonable timeframe.

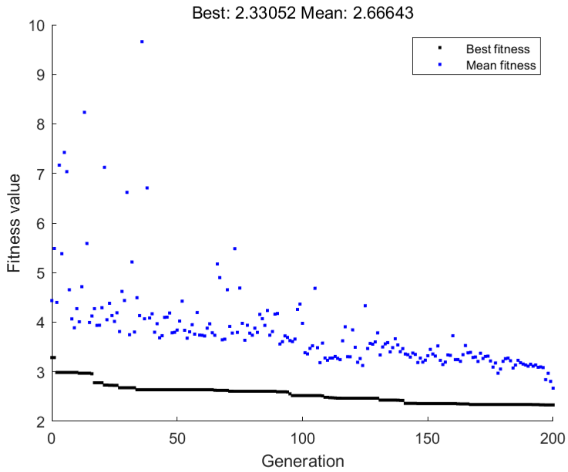

Figure 9. GA-BP model fitness.

Figure 10 illustrates the network performance and parameter changes during the training phase. The blue solid line in the figure indicates the training process, the green solid line indicates the verification process, and the red solid line indicates the testing process. After training the neural network for the seventh time, the dotted line represents the best iterative result.

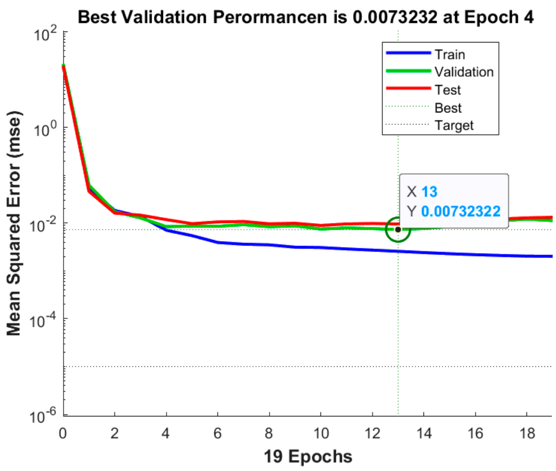

Figure 10. Training process of the GA-BP neural network.

A linear regression fitting relationship exists between the output data of the model and the target data of the training set, as shown in Figure 11. The training set was in a state of basic fit, and the (R) value was 0.989, close to 1, thus indicating a high degree of linear correlation between the two.

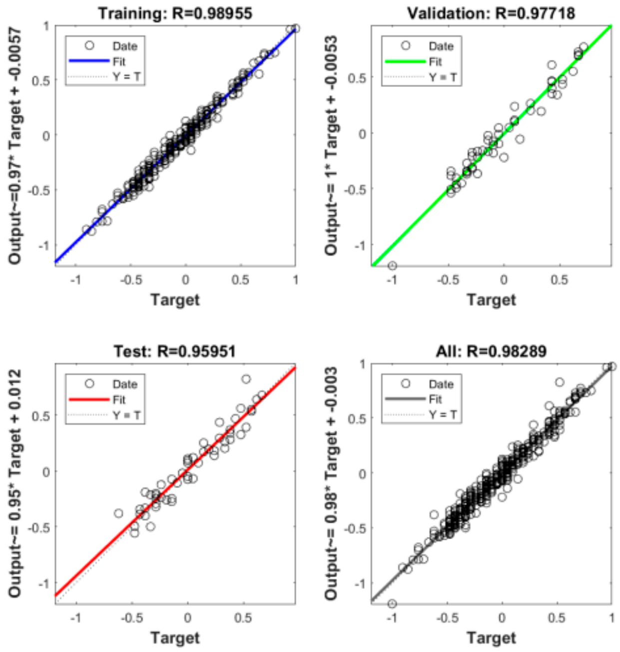

Figure 11. GA-BP regression model. The asterisk (*) indicates that the P-value of the model is less than 0.05, which proves that the model is reliable.

Linear regression and fitting were performed on the model output data and the target data of the validation set. The training set exhibited a state of basic fit, with the (R) value reaching 0.977, which is proximate to 1, thereby signifying a high degree of linear correlation between the two.

Linear regression and fitting were carried out on the model output data and the target data of the test set as well. The training set showed a state of basic fit, and its (R) value was 0.959, approaching 1 and suggesting a high level of linear correlation between them.

The linear regression fit between the model output data and the target data of the entire data set was in a basic fit state, and the (R) value was 0.982, which is close to 1, indicating a high degree of linear correlation between the two.

The model's regression results show that it fit very well: the overall fit was 0.982, and the minimum fit was 0.959. This is a high level of fit, and it is better than the BP neural network model's test results.

Figures 12 and 13 demonstrate that the test-set results of the GA-BP model closely align with those of the training set. In terms of the prediction accuracy of the actual values, the output of the model's predicted compensation value, corresponding to GA-BP, is closer to the true compensation value, corresponding to the actual sample. Moreover, compared with the traditional BP model, GA-BP had better prediction accuracy and better overall model prediction performance.

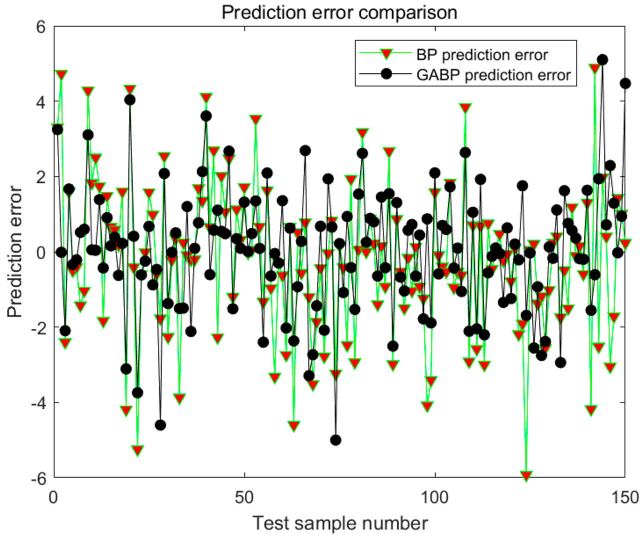

Figure 12. Absolute error of the training set.

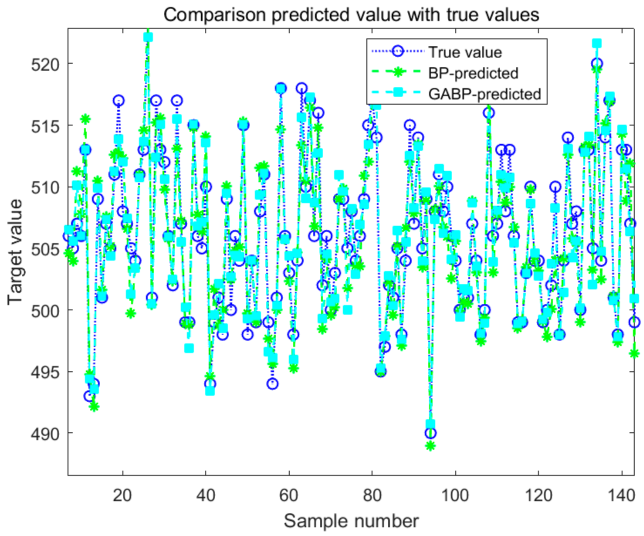

Figure 13. Test results of the training set.

Judging from the absolute error indicators corresponding to the model-predicted values and the actual compensation values, as shown in Figure 14, which is a 3D conical bar chart, the magnitude of the Y value determines the height in the Z direction. The GA-BP model significantly outperformed the BP model in all four indicators of MSE (Mean Squared Error), RMSE (Root Mean Squared Error), MAE (Mean Absolute Error), and MAPE (Mean Absolute Percentage Error). Moreover, the correlation coefficient (R) values corresponding to the GA-BP model were all greater than those of the BP model. Therefore, the overall performance of the GA-BP model was better.

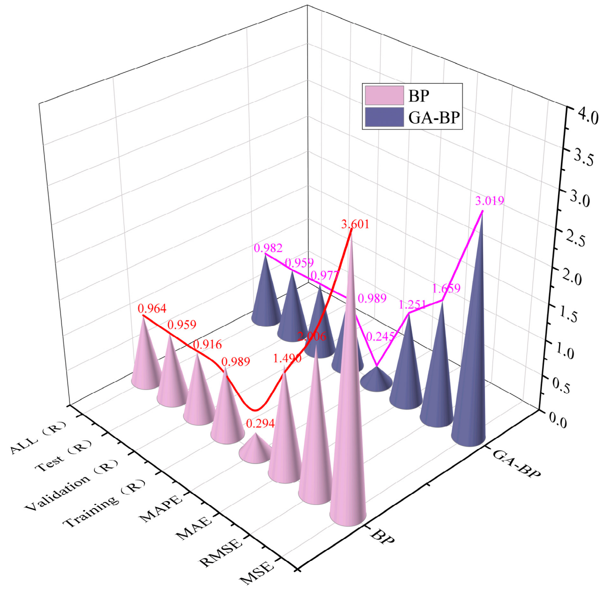

Figure 14. Comparison of data between GA-BP and BP models.

In order to more comprehensively and rigorously evaluate the performance edge of the GA-BP model, an ablation experiment was meticulously devised. In this experiment, the crossover operation was deliberately removed, and solely the mutation operation was preserved to update the individuals within the population. The code was subsequently run, and this same operation was replicated three times to ensure the reliability of the results. During each run, the MSE, RMSE, MAE, and MAPE were precisely recorded. Thereafter, the average values of these performance metrics were calculated for both models. The GA-BP model with the mutation operation intact was designated as Model B, which represents the standard GA-BP model, while the GA-BP model lacking the mutation operation was labeled as Model A. As vividly illustrated in the accompanying Figure 15, it is unmistakably evident that all four performance indicators of Model B are substantially smaller than those of Model A. This conspicuous disparity unequivocally attests to the fact that the standard GA-BP model (Model B) exhibits significantly enhanced performance, thereby further corroborating the superiority of the GA-BP model in practical applications.

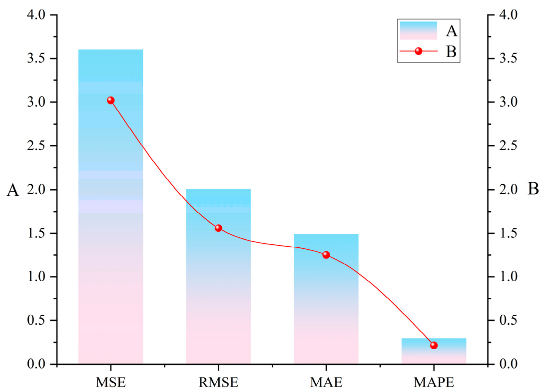

Figure 15. Comparison chart of ablation experiments for the GA—BP model.

5. Comparison of Optimization Results

The GA-BP neural network model adds the genetic algorithm to the BP neural network to make its parameters more stable and improve the accuracy of its predictions. Although it will consume more computational resources during the iteration process, the GA-BP model is a worthy choice when dealing with complex nonlinear problems. Therefore, this paper selects the GA-BP model to optimize the screw conveyance and finally obtain a fitness value of 0.007. The power consumption is $P = 0.079$ kW and the conveying capacity is $Q_m = 23.98$ t/h. The optimization results of each parameter are as follows: the outer diameter of the screw is $D = 320$ mm, the pitch is $S = 200$ mm, and the rotational speed of the pickup shaft is $n = 138$ r/min. Figure 16 shows a comparison between the optimization results of the objective function and the parameters of mainstream domestic straw balers. (The parameters of the mainstream models for comparison mainly come from the official data of the China Agricultural Machinery Network).

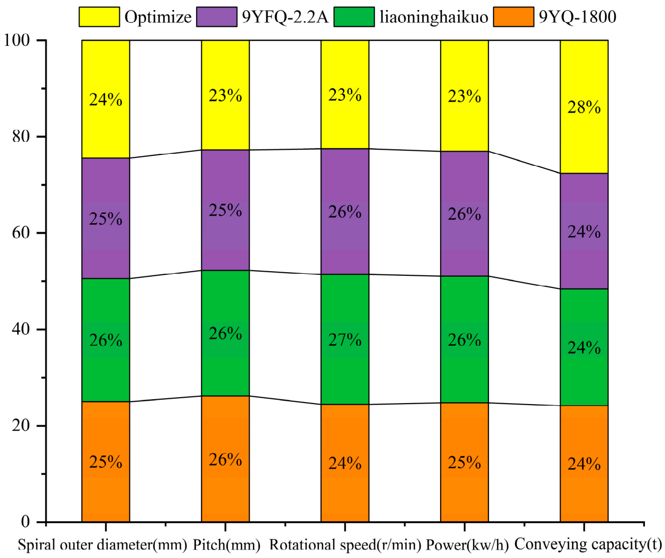

Figure 16. Comparison of optimized parameter results.

The figure is a chart showing the spiral conveying parameters of several popular balers as well as the proportion of the optimized parameters. In the figure, the yellow part represents the proportion of optimized parameters in the GA-BP model. The power consumption proportion, at 23%, is the lowest among the four combinations, while the feeding amount proportion, at 28%, is the highest. The spiral conveying performance has improved compared to other models, as this optimization meets the conditions of the highest conveying amount and the lowest power. Therefore, this optimization is effective.

6. Experiment

In the actual operation of balers, numerous factors can exert an impact on the baling process. Conducting field tests with the whole machine fails to precisely explore the performance of the spiral conveyor. Consequently, a spiral conveyor was employed to conduct the planned experiment, which enabled the verification of the efficacy of the optimal set of parameters and enhanced the accuracy and reliability of the test data. Colored balls were utilized as substitutes for straws(As shown in Figure 17). The test parameters are presented in the Table 4, and the parameters of the control group correspond to the spiral conveying parameters of mainstream domestic straw balers as listed in Section 5.

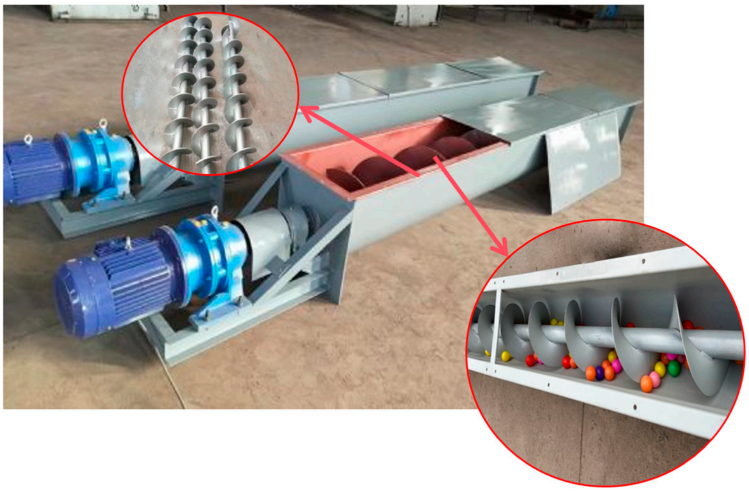

Figure 17. Comparative tests on screw conveying.

Table 4. Test Parameter Settings.

Characteristic	Experimental Group X_1	Control Group X_2	Control Group X_3	Control Group X_4
Rotational speed of the screw shaft (rad/min)	138	160	160	140
Outer diameter of the Screw (mm)	320	300	320	300
Pitch (mm)	200	240	200	190

For the experiment, two control groups were established to verify the performance of the model's optimally combined prediction. The model predicted that for test group X_1, which represents the optimized spiral conveying structure, the optimal result will pertain to the rotational speed of the screw shaft. These three groups employed the spiral conveying parameters of two of the most prevalent balers in the market, namely the 9YQ —1800 and the 9YFQ—2.2A. Their corresponding test numbers are X_2, X_3, and X_4 in sequential order. A working time of 1 h was stipulated, following which the consumed power was calculated. The mass of the small balls was used as a substitute for the conveyed amount.

The efficiency of spiral conveying is represented by η. Specifically, $\eta = \frac{Q_m}{P}$ was used to sort out the obtained data and plot them as shown in the figure.

In Figure 18, the green solid line represents the curve of the optimized screw conveying efficiency. The other three solid lines with different colors almost overlap, indicating that their slopes are basically the same; that is, there is little difference in efficiency η.

The fact that the slope of the green solid line is significantly greater than that of the other three solid lines serves as an indication that its corresponding efficiency is the largest. Subsequently, it can be concluded that the efficiency η is superior to that of other combinations, which in turn verifies the validity of the model's prediction results.

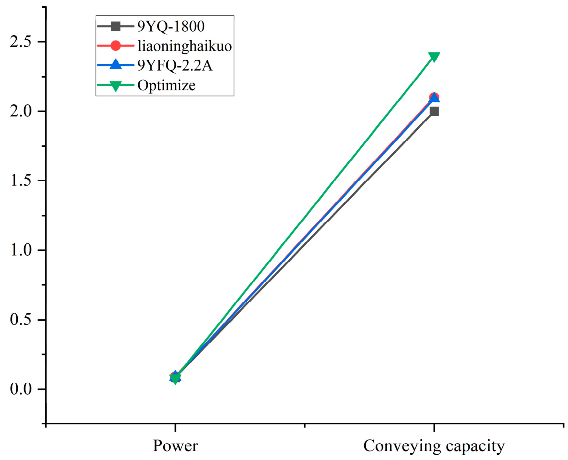

Figure 18. Comparison of experimental results.

7. Conclusions

This paper provides a brief explanation of the baler's working principle and conducts an analysis of the force conditions and velocity components of the straw during its conveyance by the screw conveyor. The analysis establishes a mathematical model to determine the parameters influencing screw conveying efficiency, elucidates the design principles of these parameters, and employs MATLAB (R2023a) software for optimization programming. Since the BP neural network model is prone to extremely slow convergence or failure to converge due to getting trapped in local minima, a genetic algorithm was selected to optimize the BP neural network model. Subsequently, the optimization results were compared with those of mainstream models on the market. Finally, experiments were carried out to verify the optimization results, and the following conclusions were drawn:

1. The main factors influencing screw conveying efficiency are primarily pitch, the rotational speed of the screw shaft, and the outer diameter of the screw. The constraint conditions were determined through calculations;
2. To optimize the screw conveying parameters, the BP and GA-BP models were established separately. According to the results, the GA-BP model demonstrated superior performance in terms of MSE (Mean Squared Error), RMSE (Root Mean Squared Error), MAE (Mean Absolute Error), MAPE (Mean Absolute Percentage Error), and the corresponding correlation coefficient (R) values compared to the BP model;
3. The optimal parameters for screw conveyance have been obtained. Specifically, the outer diameter of the screw is $D = 320$ mm, the pitch is $S = 200$ mm, and the rotational speed of the picking-up shaft is $n = 138\ r/\text{min}$. Under these conditions, the minimum power consumption $P = 0.079$ kw and the maximum conveying capacity $Q_m = 23.98$ t/h are achieved;
4. The outcomes of the comparative experiments indicate that the screw conveying efficiency after optimization is conspicuously superior to that of other mainstream balers. This further validates the reliability of the predictions yielded by the GA-BP model, and its resultant data can provide a valuable reference for the research on the screw conveying structure of balers.

8. Prospect

This research endeavor might have predominantly centered around the immediate enhancement of performance subsequent to optimization, yet it has fallen short in carrying out long-term stability and reliability tests on the optimized screw conveying apparatus. Over an extended operational period, critical aspects such as the fatigue of components, loosening phenomena, and the progressive alteration of performance have not been exhaustively investigated. Such investigations are of fundamental significance for ensuring the seamless and efficient functioning of the equipment within the context of actual production. Moreover, notwithstanding the attainment of the optimization objectives, namely maximizing the conveying volume and minimizing power consumption, a host of other pivotal factors in practical applications cannot be overlooked. These encompass equipment costs, the ease of maintenance, noise levels, and so forth, all of which merit equal attention as they could substantially influence the overall viability and applicability of the device in real-world scenarios.

Author Contributions: Conceptualization, Q.G.; methodology, Y.Z.; software, H.X.; investigation, Z.W.; writing—original draft preparation, Y.Z.; writing—review and editing, Q.G.; visualization, W.L.; project administration, H.L. All authors have read and agreed to the published version of the manuscript.

Funding: This work was supported by special funds for basic scientific research of universities from the Education Department Heilongjiang Province (145309613), Heilongjiang Higher Education Teaching Reform Project (SJGY20220410), and key projects of Heilongjiang's education science planning (GJB1422296).

Institutional Review Board Statement: Not applicable.

Data Availability Statement: Data are reported within the article.

Conflicts of Interest: The authors declare no competing interests.

References

1. Duan, J.; Cheng, F.; He, C.; Liu, Y.; Wang, Y.; Guo, X. Research status and development trend of medium and small silage maize harvesters. *J. Chin. Agric. Mech.* **2024**, *45*, 305–310.
2. Pal, R.; Kumar, R.; Jalal, R.K.; Kumar, A. Economic and Environmental Performace of Straw Baler for Collection of Rice Residue Generated after Mechanical Harvesting by Combine Harvester. *Curr. J. Appl. Sci. Technol.* **2019**, *37*, 1–6. [CrossRef]
3. Kiani, F.; Randazzo, G.; Yelmen, I.; Seyyedabbasi, A.; Nematzadeh, S.; Anka, F.A.; Erenel, F.; Zontul, M.; Lanza, S.; Muzirafuti, A. A Smart and Mechanized Agricultural Application: From Cultivation to Harvest. *Appl. Sci.* **2022**, *12*, 6021. [CrossRef]
4. da Silveira, F.; Machado, F.M.; Romano, L.N.; Amaral, F.G.; Ruppenthal, J.E. Strategy for the development of agricultural machinery: Importance of patent analysis. *Braz. J. Oper. Prod. Manag.* **2018**, *15*, 535–544. [CrossRef]
5. Thomas, G.; Balocco, S.; Mann, D.; Simundsson, A.; Khorasani, N. Intelligent Agricultural Machinery Using Deep Learning. *IEEE Instrum. Meas. Mag.* **2021**, *24*, 93–100. [CrossRef]
6. Wang, J.; Zeng, F.; Cui, J.; Bai, H.; Li, X.; Zhao, Z. Design and Experiments of the Data Acquisition System for Bale Rolling Characteristic Parameters on a Large-Scale Round Bale Machine. *Processes* **2024**, *12*, 1042. [CrossRef]
7. Wang, Q.; Jiang, Y.; Li, L.; Qin, J.; Chen, L. Performance analysis of a spring-tooth drum pickup of straw baler via coupling simulation. *Int. J. Agric. Biol. Eng.* **2021**, *14*, 159–165. [CrossRef]
8. Tang, Z.; Zhang, B.; Liu, X.; Ren, H.; Li, X.; Li, Y. Structural model and bundling capacity of crawler picking and baling machine for straw wasted in field. *Comput. Electron. Agric.* **2020**, *175*, 105622. [CrossRef]
9. Kalay, E.; Bogoclu, M.E.; Bolat, B. Mass flow rate prediction of screw conveyor using artificial neural network method. *Powder Technol.* **2022**, *408*, 117757. [CrossRef]
10. Zhao, Z.; Huang, H.; Yin, J.; Yang, S.X. Dynamic analysis and reliability design of round baler feeding device for rice straw harvest. *Biosyst. Eng.* **2018**, *174*, 10–19. [CrossRef]
11. Hu, B. Design and Testing of The Long Seedling Transport and Collection Device for Peanut Picking and Harvesting Machines. Master's Thesis, Henan Agricultural University, Zhengzhou, China, 2023.
12. Li, G.; Ma, J.; Tian, X.; Zhao, C.; An, S.; Guo, R.; Feng, B.; Zhang, J. Discrete Meta-Simulation of Silage Based on RSM and GA-BP-GA Optimization Parameter Calibration. *Processes* **2023**, *11*, 2784. [CrossRef]
13. Tian, Y.; Yuan, P.; Yang, F.; Gu, J.; Chen, M.; Tang, J.; Su, Y.; Ding, T.; Zhang, K.; Cheng, Q. Research on the Principle of a New Flexible Screw Conveyor and Its Power Consumption. *Appl. Sci.* **2018**, *8*, 1038. [CrossRef]
14. Desnica, E.; Asonja, A.; Mikic, D.; Stojanovic, B. Reliability model of bearing assembly on an agricultural cardan shaft. *J. Balk. Tribol. Assoc.* **2015**, *21*, 38–48.

15. Ašonja, A.; Adamović, Ž.; Jevtić, N. Analysis of reliability of cardan shafts based on condition diagnostics of bearing assembly in cardan joints. *Metal. Int.* **2013**, *18*, 216–221.
16. WuLan, T.; Wang, C.; Zhao, F.; Wang, X. Experiment and optimization of screw conveyor parametersfor rubbing and breaking corn straw. *J. China Agric. Univ.* **2019**, *24*, 115–122.
17. Gao, L.; Liang, G.; Cai, Y.; Feng, W.; Yang, Y.; Liu, J.; Yang, J. Pickup device with shovel teeth and double cylindersfor the bunch ofpeanuts. *Trans. Chin. Soc. Agric. Eng.* **2024**, *40*, 13–22.
18. Liao, P.; Zhuo, D.; Fu, C.; Liu, K.; Zhang, A.; Gong, C. Improve design and test of selfpropelled cotton stalk combine harvest baler. *J. Chin. Agric. Mech.* **2021**, *42*, 19–25.
19. Lin, J.; Liao, Q.; Wang, X.; Kang, Y.; Du, W.; Zhang, Q. Exploring straw movement through the simulation of shovel-type seedbed preparation machine-straw-soil interaction using the DEM-MBD coupling method. *Comput. Electron. Agric.* **2024**, *226*, 109465. [CrossRef]
20. Guo, X.; Wang, Z.; Wang, X.; Zhao, X.; Wang, Q.; Bao, Z.; Gao, L.; Wang, J. Improvement of Pickup and Feeding System of Baler Based on TRIZ Theory. *Agric. Eng.* **2022**, *12*, 87–89.
21. Sun, H.; Ma, H.; Zhao, Y. DEM investigation on conveying of non-spherical particles in a screw conveyor. *Particuology* **2022**, *65*, 17–31. [CrossRef]
22. Zhang, H.; Li, Z.; Yang, Z.; Zhu, C.; Ding, Y.; Li, P.; He, X. Detection of the Corn Kernel Breakage Rate Based on an Improved Mask Region-Based Convolutional Neural Network. *Agriculture* **2023**, *13*, 2257. [CrossRef]
23. Zhang, L.; Wang, F.; Sun, T.; Xu, B. A constrained optimization method based on BP neural network. *Neural Comput. Appl.* **2018**, *29*, 413–421. [CrossRef]
24. Jiang, H.; Yu, Z.; Wang, Y.; Zhang, B.; Song, J.; Wei, J. The state prediction method of the silk dryer based on the GA-BP model. *Sci. Rep.* **2022**, *12*, 14615. [CrossRef] [PubMed]
25. Dao, S.D.; Abhary, K.; Marian, R. An innovative framework for designing genetic algorithm structures. *Expert Syst. Appl.* **2017**, *90*, 196–208. [CrossRef]
26. Aschenbrenner, E.; Funke, A. Numerical Validation of a Screw Conveyor Design Method. *Energy Fuels* **2024**, *38*, 13019–13028. [CrossRef]
27. Jia, D.; Zheng, W.; Wei, X.; Guo, W.; Zhao, Q.; Gao, G. Parametric Design and Genetic Algorithm Optimization of a Natural Light Stereoscopic Cultivation Frame. *Agriculture* **2024**, *14*, 84. [CrossRef]
28. Chen, F.; Zhang, Q.; Chen, S.; Yuan, Y. Research on Operation Efficiency Prediction and Optimization of Biological Retention System Based on GA-BP Neural Network Model. *Sustainability* **2023**, *15*, 10990. [CrossRef]
29. Liu, M.; Ma, X.; Feng, W.; Jing, H.; Shi, Q.; Wang, Y.; Huang, D.; Wang, J. Optimization of Operation Parameters and Performance Prediction of Paddy Field Grader Based on a GA-BP Neural Network. *Agriculture* **2024**, *14*, 1283. [CrossRef]